Chapter 6

Molecular processes of Fluoromethanes for wide energy range

Present section reports the electron collision study of fluoromethanes (CH_2F_2 and CH_3F) for the broad energy spectrum from 0.1 to 5000 eV. Through R-matrix approach, the low energy calculations (from 0.1 to 20 eV) are performed. High energy computations (from ionisation threshold to 5 keV) are accomplished through SCOP and CSP-ic methodology. Various cross-sections, viz., differential cross-section (Q_{EDCS}), momentum-transfer (Q_{MTCS}), Q_{el}, Q_{inel}, Q_{ion} and ΣQ_{exc} are computed for the electron interaction with CH_2F_2 molecule.

6.1 Introduction

In recent years, a significant amount of research effort has been focused on the study of electron interaction with the fluoromethanes. Plasma processing, environmental research fields, material science, all place a significant emphasis on the electron collision cross sections of these molecules [1,2]. Although these species contribute to the global warming process, they are pointed out as "ecofriendly, next-generation plasma-processing gases" and are therefore possible replacements for CF_4 in plasma processing.

In high-energy systems, where rapid molecular energy transfer or effective surface chemical attack are priorities, the fluoromethane molecular family's unique combination of characteristics comes in demand. Also, it is widely known that fluoromethanes play a significant part in the process of etching semiconductors as well as in the ionosphere that surrounds the earth [3].

Thus, present research work has been chosen to study the electron collisions with the fluoromethanes (CH_2F_2 and CH_3F) over a broad range of energy, i.e., from 0.1 eV to 5000 eV by employing two methodologies: a) R-matrix and b) SCOP in conjunction with CSP-ic.

6.2 Difluoromethane (CH_2F_2)

The effects of global warming pose one of the greatest threats to humanity today. In addition to naturally occurring greenhouse gases such as methane, carbon dioxide, and nitrous oxide, man-made greenhouse gases such as hydrofluorocarbons (HFCs) and perfluorocarbons (PFCs) play a major part in the global warming process [4,5]. These chemicals also have exceptionally long atmospheric half-lives, which causes an accumulating in the atmosphere that is almost impossible to reverse [6].

To replace the stratospheric ozone-depleting chemicals chlorofluorocarbons (CFCs) and hydrochlorofluorocarbons (HCFCs), which are currently being phased out in compliance with the Montreal Protocol on substances that deplete the ozone layer, HFCs have been developed. HFCs are exclusively anthropogenic substances. Their primary uses are as propellants for aerosols, insulating foams, refrigeration, and air conditioning systems. In the 1990s, HFCs began to be commercialised. Given that they have an atmospheric lifespan of 15–29 years, HFCs are among the most powerful greenhouse gases [7].

Difluoromethane (CH_2F_2), often referred to as HFC-32, has no ozone depletion potential (ODP) and an atmospheric lifetime of about 5 years [8]. According to the GHG Protocol 2016 [9], HFC-32 has an estimated 677 GWP over a 100-year timeframe. HFC-32 is a safe alternative to other HFCs due to its high GWP and longer leak persistence. CH_2F_2 is an efficient refrigerant molecule for both vaporisation and condensation in terms of pressure drop and heat transmission [10]. In Japan, China, and India, difluoromethane is used in air conditioners as an alternative to R-410A [11]. They are among the greenhouse gases with the greatest rate of growth because of the rising demand for refrigeration and air conditioning, particularly in emerging nations [11]. CH_2F_2 is commonly employed as a fire extinguishant because it can undergo endothermic reactions [12]. It can also be used as a solvent, blowing agent, and aerosol propellant [11,13].

In the microelectronic industries, CH_2F_2 (one of the fluorocarbons) is also utilised for dry etching of silicon wafers and dielectric thin films (SiO_2, Si_3N_4) [14,15]. The low dielectric constant of fluorocarbon films makes them promising ILD (interlayer dielectric) materials. By lowering power consumption (i.e., $\propto CV^2$), propagation delay (i.e., the RC time constant), and cross-coupling noise between adjacent lines, they made it possible to achieve greater performance with fewer design constraints. Fluorocarbon films produced by plasma-enhanced chemical vapour deposition (PECVD) have been the subject of extensive investigation [16].

Therefore, in the present study, we have taken into account CH_2F_2, one of the fluoromethanes (fluorocarbons or HFCs), and reported various electron interaction cross-sections for a wide energy range of 0.1 eV to 5000 eV.

6.2.1 Literature study

Table 6.1 is a compilation of all existing cross-section data for a better understanding. According to the literature study, experimental data of electron cross-section are quite scarce and also energy-fragmented when compared to theoretical cross-section values.

Table 6.1 Literature survey on e^- - CH_2F_2 scattering study

Quantity	Energy (eV)	Method of investigation		Reference
		Theoretical	Experimental	
Q_T	100-1500	Revised additivity rule	-	Tan *et.al.* [17]
	500-10000	Using semi-empirical formula	-	Manero *et.al.* [18]
	100-3000	Additivity rule (AR) method	-	Jin-Feng *et.al.* [19]
	30-5000	Geometric additivity rule	-	Shi *et.al.* [20]
	0-1000	Obtained from Sueoka group	-	Kimura *et.al.* [21]
Q_{el}	0-15	Schwinger multi-channel method (SMC)	-	Varella *et.al.* [22]
	500-10000	Using semi-empirical formula	-	Manero 2002 [18]
	0-1000	Obtained from Sueoka group	-	Kimura *et.al.* [21]

		Sueoka et.al. data		
Vibrational Q_{el}	3-30	Using fixed-nuclei approach in general theory of scattering	-	Nishimura *et.al.* [23]
Q_{EDCS}	0-15	Schwinger multi-channel method (SMC)	apparatus of the crossed-beam type using the relative flow technique [15-20%]	Varella *et.al.* [22]
	At 20	Schwinger multi-channel method (SMC)	-	Natalense *et.al.* [24]
	1.5-100	Continuum multiple scattering (CMS) method	apparatus of the crossed-beam type using the relative flow technique [15-30% error]	Tanka *et.al.* [2]
	At 10 and 30	Schwinger multi-channel method (SMC)	-	Natalense *et.al.* [25]
Vibrational Q_{EDCS}	3-30	Using fixed-nuclei approach in general theory of scattering	-	Nishimura *et.al.* [23]
Q_{MTCS}	1.5-15	Schwinger multi-channel method (SMC)	-	Varella *et.al.* [22]
	10-30	Schwinger multi-channel method (SMC)	-	Natalense *et.al.* [24]
Vibrational Q_{MTCS}	3-30	Using fixed-nuclei approach in general theory of scattering	-	Nishimura *et.al.* [23]
Q_{inel}	500-10000	Using semi-empirical formula	-	Manero *et.al.* [18]
Q_{ion}	0-100	-	crossed-beam collisions analysed by time-of-flight mass spectroscopy (TOF-MS)	Torres *et.al.* [26]
	10-1000	Review data	-	Karwasz *et.al.* [27]
	10-500	BEB/ DM/ modified additivity rule/ HV (Harland and Vallance)	-	Torres *et.al.* [28]
	IE-5000	CSP-ic approach	-	Verma *et.al.* [29]

6.2.2 Target model

For the purpose of computing electron interactions with CH_2F_2 at low energy, the R-matrix formalism using Quntemol-N code is employed. Three scattering models, viz., SE, SEP and CI are employed in this study, with 6-311G* basis set. Since CH_2F_2 has a 1.970 debye, permanent dipole moment, more partial waves, i.e., $l > 4$ are required for the convergence. Thus, born correction [30,31] is applied to all energies, increasing the Q_{el}, specifically at lower energy regime.

Table 6.2 shows various target properties of CH_2F_2 that were estimated using three distinct scattering models (SE, SEP, and CI).

Table 6.2 Various target properties of CH_2F_2 calculated using Quantemol-N

Target properties (unit)		Present (Quantemol-N/6- 311G*)			Others	
		CAS-CI	SE	SEP	Theoretical	Experimental
Ground state energy (Hartree)		-237.9598	-237.9583	-237.9583	-237.8687 [32] -238.0119 [23]	-
Dipole moment (Debye)		1.970	1.970	1.970	2.0561 [23]	1.970 [33]
Rotational constant (cm^{-1})	A	1.7415	1.7415	1.7415	1.6219 [34] 1.6392 [35] 1.6381 [36]	1.5921 [33]
	B	0.3564	0.3564	0.3564	0.3455 [34] 0.3537 [35] 0.3535 [36]	0.3538 [33]
	C	0.3139	0.3139	0.3139	0.3019 [34] 0.3085 [35] 0.3083 [36]	0.3085 [33]

The ground state energy of CH_2F_2 agrees well with that Brundle *et.al.* [32] and Nishimura [23]. Rotational constants derived using the current models are found to be marginally higher than theoretical [34–36] and experimental [33] values. However, the current computed dipole moment is in perfect agreement with the experimental value [33] and in good accord with that of Nishimura [23]. As a result of the good agreement of molecular properties estimated here, the current scattering models are appropriate for the present study on CH_2F_2.

The target parameters which are used in the calculation of high energies through SCOP, are listed below in table 6.3.

Table 6.3 Properties of CH_2F_2 [33]

Properties	Values
Ionisation energy (eV)	12.71
Polarisability ($Å^3$)	2.76
Bond length (Å)	C-H = 1.0840 C-F = 1.3508

CH_2F_2 is a C_{2v} symmetric tetrahedral molecule. The HF ground state electron configuration for CH_2F_2 employed in this study is $1(b_2)^2$, $1(a_1)^2$, $2(a_1)^2$, $3(a_1)^2$, $2(b_2)^2$, $4(a_1)^2$, $1(b_1)^2$, $5(a_1)^2$, $3(b_2)^2$, $1(a_2)^2$, $4(b_2)^2$, $6(a_1)^2$, $2(b_1)^2$. All 26 electrons are rendered inactive in the lowest setting of the SEP and SE model. For the augmentation of the continuum orbitals in the SE model, the computations incorporate 1 virtual molecular orbital (MO) of each A_1, B_1, and B_2 symmetry. For augmentation of the continuum orbitals, the SEP model, on the other hand, retains 19 MOs of A_1, 10 MOs of B_1, 13 MOs of B_2, and 5 MOs of A_2. In the CI, however, 18 of the 26 electrons are kept frozen in positions $1a_1$, $2a_1$, $3a_1$, $4a_1$, $5a_1$, $1b_1$, $1b_2$, $2b_2$, and $3b_2$. The remaining 8 electrons are free to move in the active space of the 6 molecular occupied and virtual orbitals $6a_1$, $7a_1$, $2b_1$, $3b_1$, $4b_2$, $5b_2$, and $1a_2$. Four MOs are assigned to improve the continuum orbitals, three of which retain A_1 symmetry and one of which retains B_1 symmetry. To obtain more precise calculations, for ground state representation, 523 configuration state functions (CSFs) and for close coupling expansion and outer regime calculation, 11 target states are used. The first 11 excited states are tabulated in Table 6.4 for CH_2F_2 molecule.

Table 6.4 Vertical excitation energies for all states of CH_2F_2

	States	Energy (eV)
Singlet	A_1	0
Triplet	B_1	12.2309
Singlet	B_1	12.5629
Triplet	A_2	13.2431
Triplet	A_1	13.3275
Singlet	A_2	13.7601

Singlet	A_1	14.1274
Triplet	A_1	14.8621
Singlet	A_1	15.0798
Triplet	B_2	15.1097
Singlet	B_2	15.5478

6.2.3 Results and Discussion

In order to provide a full database, we conducted an elaborative investigation on the electron collision cross-section for the CH_2F_2 molecule for 0.1 eV to 5000 eV impact energies. We employed the ab-initio R-matrix technique for low energy studies ranging from 0.1 to 20 eV and reported Q_{el}, Q_{EDCS}, and Q_{MTCS}. The SCOP formalism is used to derive the Q_{inel}, Q_{ion}, Q_{exc} and Q_T from the ionisation energy to 5000 eV.

A. Low energy results

Figure 6.1 displays the eigen phase sum for the e^- - CH_2F_2 collision, which contains information on the resonance widths and position. Resonance is an ordinary phenomenon of electron molecule interaction at low energies. The incoming electron is captured by the target molecule in the interim during a transient negative ion resonance, resulting in a sharp pattern in the cross- sections at a given incident energy.

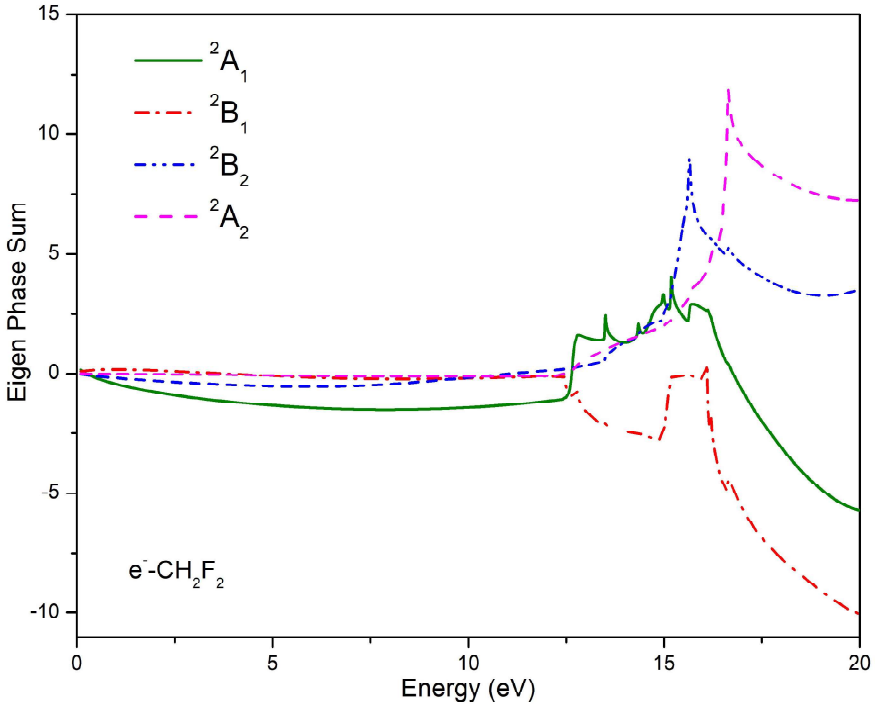

Figure 6.1 Eigen phase sum for $e^- - CH_2F_2$ scattering

Green solid: $^2A_1$ symmetry state; red dash dot: $^2B_1$ symmetry state; blue dash dot dot: $^2B_2$ symmetry state; magenta dash: $^2A_2$ symmetry state

A full description of dissociative electron attachment (anion) is the formation of a compound state represented by the resonance, which thereafter decays either by spontaneous detachment or by dissociating the molecule to generate a neutral atom and a negative ion. As a result, it contributes to the study of molecular disintegration processes. The eigen phase sum results for the four symmetry states ($^2A_1$, $^2B_1$, $^2B_2$ and $^2A_2$) of the CH_2F_2 molecule produced from the CI model are shown in Figure 6.1. We used an iterative approach for discovering and executing Breit-Wigner fits to the eigen phase diagram with the programme RESON to calculate the positions and widths of resonances [37].

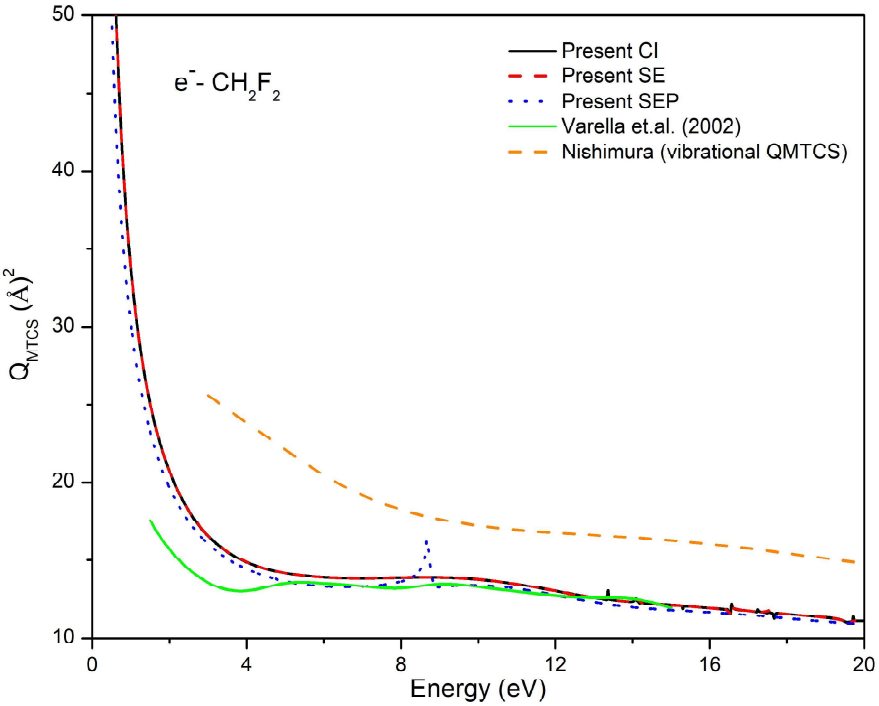

Figure 6.2 Q_{MTCS} for $e^- - CH_2F_2$ scattering

Black solid: Present CI result; red dash: Present SE result; blue dot: Present SEP result; green solid: Varella et.al. [22]*; orange dash: vibrational Q_{MTCS} results by Nishimura* [23]

The Q_{MTCS} is the most important input measure used to solve the Boltzmann equation for plasmas and gases [38]. The Q_{MTCS} is obtained by multiplying the integrated differential cross-sections by a factor of (*1-cosθ*). Figure 6.2 compares the current Q_{MTCS}, computed using three distinct models: SE, SEP, and CI, to the data of Varella *et.al.* [22] and Nishimura [23] for energies ranging from 0.1 to 20 eV. The current data is in good accord with that of Varella *et.al.* [22]. The vibrationally elastic Q_{MTCS} reported by Nishimura [23] is likewise compared here, and it overestimates the current Q_{MTCS}.

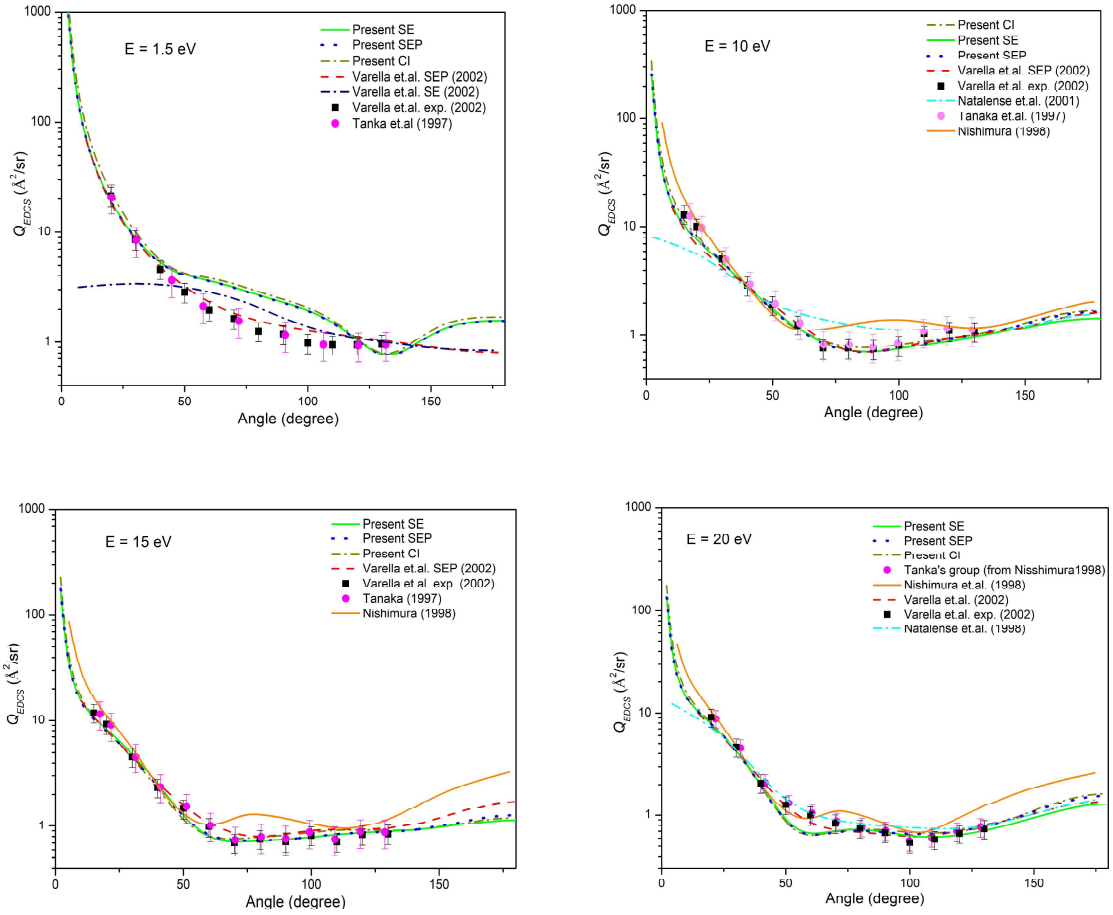

Figure 6.3 Q_{EDCS} for energies 1.5 eV, 10 eV, 15 eV, and 20 eV

Green solid: Present Q_{EDCS} (SE model); blue dot: Present Q_{EDCS} (SEP model); dark yellow dash dot: Present Q_{EDCS} (CI model); red dash: Varella et.al. calculated Q_{EDCS} [22]*; filled squares: Varella et.al. measured Q_{EDCS}* [22]*; filled circles: Tanaka et.al.* [2]*; cyan dash dot: Natalense et.al.* [24,25]*; orange solid: Nishimura* [23]

Figure 6.3 depicts the present Q_{EDCS} data for CH_2F_2 for energies of 1.5 eV, 10 eV, 15 eV, and 20 eV. The Q_{EDCS} of CH_2F_2 continues to rise rapidly at small angles, resulting in a noticeable forward peak, a feature due to the polar molecules' long-range dipole interactions. At the energy of 1.5 eV, the only existing data for Q_{EDCS} are of Varella *et.al.* [22] and Tanaka *et.al.* [2]. Varella *et.al.* provided both experimental and calculated Q_{EDCS} results for two different approximations: SE and SEP with Born correction. The current data is consistent with the experimental results of Varella *et.al.* [22] within the specified uncertainty range of ±15-20% for $\theta < 50°$ and $120° < \theta < 135°$. Varella *et.al.* [22] theoretical data utilising the SE technique

has lower values than the current ones at forward angle regime. They also [22] underestimate the findings calculated using the SEP technique. At the intermediate angle, however, the current data follows a similar trend to that of Varella *et.al.* using the SE approximation [22]. The current Q_{EDCS} data overestimates Tanaka *et.al.* experimental results (which are not rotationally resolved) by ±15-30% [2].

However, for higher energies of 10 eV, 15 eV, and 20 eV, the current values of Q_{EDCS} correspond well with the results of Varella *et.al.* [22] and Tanaka *et.al.* [2]. Nishimura's results [23] indicate some inconsistencies with the current ones for all energies. This is due to the fact that current Q_{EDCS} data are rotationally resolved, whereas Nishimura reported vibrational Q_{EDCS} while keeping the rotational state $(j\tau) = (00)$ fixed [23]. Natalense *et.al.* [24,25] data for energies of 10 eV and 20 eV underestimates the current ones at small angles (i.e., $\theta < 20°$). The explanation for this mismatch is that Natalense *et. al.* [24,25] did not account for the polarisation effect, despite the fact that CH_2F_2 has a permanent dipole moment of 1.970 debye, which has the main influence in Q_{EDCS} at small angles, as previously indicated.

Furthermore, the 1.5 eV figure displays a broad minimum at 132°, indicating the presence of *p*-wave structure, which is absent in all of the data of Varella *et. al.* [22] and Tanka *et. al.* [2]. The 10 eV plot reveals the minima at around 82°, while the 15 eV curve displays two minima with the *d*-wave structure at around 63° and 121°. A similar characteristic can be found in the 20 eV plot, with two shallow minima at 58° and 102°.

Figures 6.4 to 6.6 depict the computed elastic cross-sections of CH_2F_2 scattering by electrons for lower energy range of 0.1 to 20 eV by using the three mentioned models (SE, SEP, and CI). In figure 6.4, the current Q_{el} results with and without born closure, derived using SE approximation, are shown against the existing data of Varella *et.al.* who utilised same scattering model [22] in the Schwinger multi-channel method. Present without born closure data is shown in excellent agreement with Varella *et.al.* [22]. However, the present result with born correction exaggerates that of Varella *et.al.* [22], but qualitatively mimics it well. The same nature of the present results with born and without born correction and those of Varella *et.al.* [22] can also be found in the case of SEP model (figure 6.5).

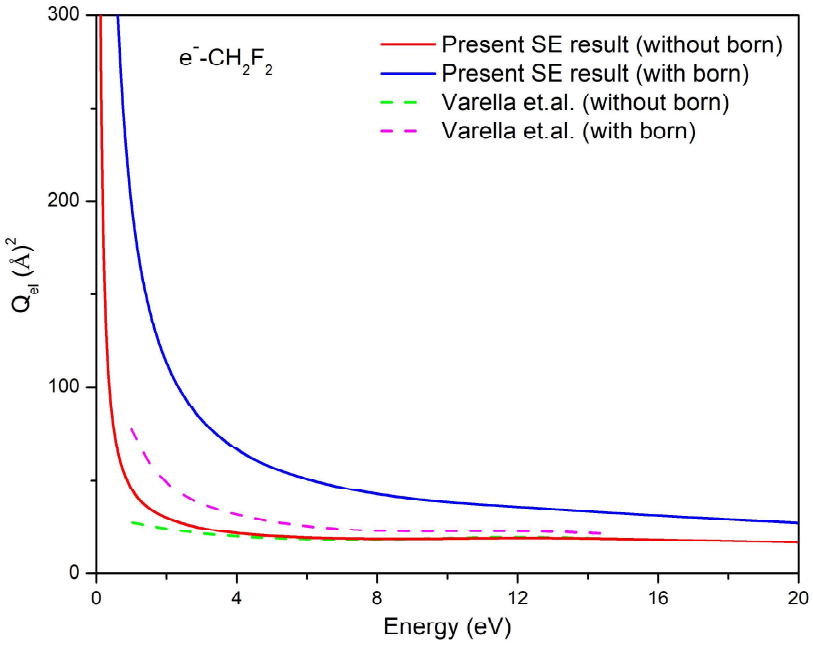

Figure 6.4 Q_{el} for $e^- - CH_2F_2$ scattering using SE model

Blue solid: Present Q_{el} (with born); magenta dash: Varella et.al. (with born); red solid: Present Q_{el} (without born); green dash: Varella et.al. (without born)

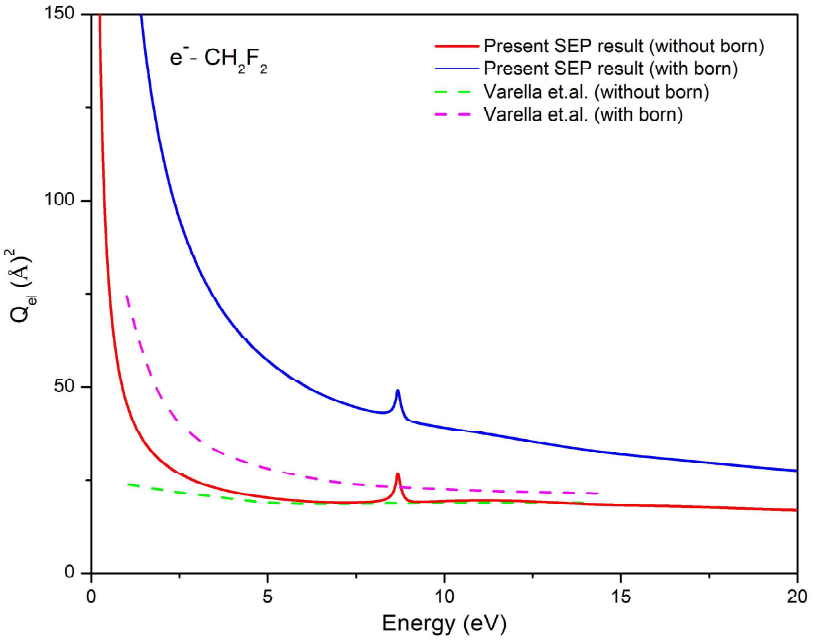

Figure 6.5 Q_{el} $e^- - CH_2F_2$ scattering using SEP model

Blue solid: Present Q_{el} (with born); magenta dash: Varella et. al. (with born) [22]; *red solid: Present Q_{el} (without born); green dash: Varella et. al. (without born)* [22]

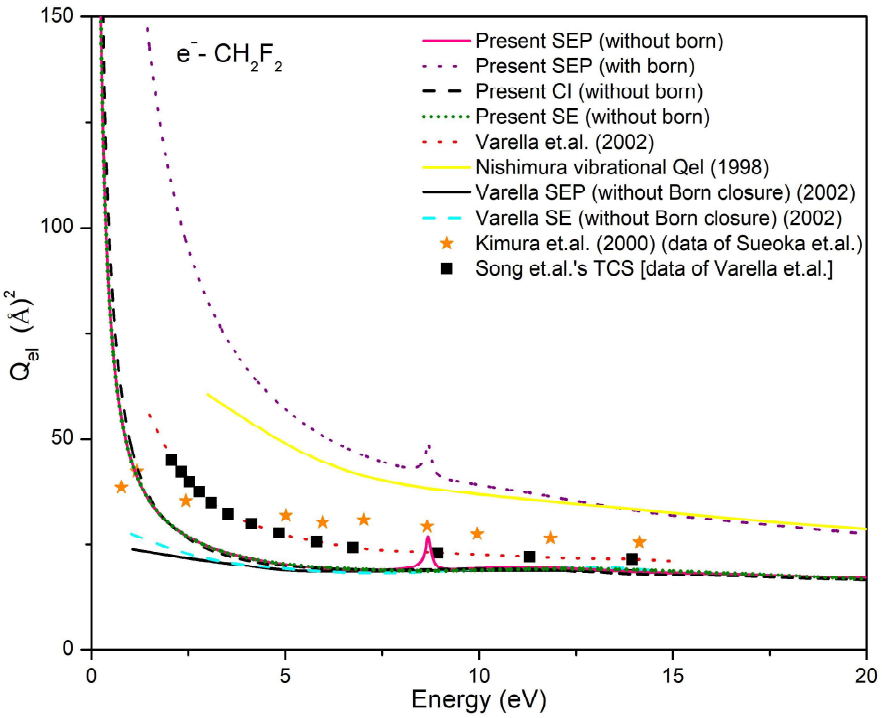

Figure 6.6 Q_{el} $e^- - CH_2F_2$ scattering

Pink solid: Present Q_{el} (SEP model without born); purple dot: Present Qel (SEPmodel with born); black dash: Present Q_{el} (CI model without born); olive green short dot: Present Q_{el} (SE model without born); red dot: Varella et.al. [22]*; yellow solid: Nishimura vibrational Q_{el}* [23]*; black solid: Varella et.al. Q_{el} (SEP model)* [22]*; cyan dash: Varella et.al. Q_{el} (SE model)* [22]*; orange stars: Kimura et.al.* [21]*; filled squares: Song et.al.* [39]

Figure 6.6 depicts the common curve of Q_{el}, which was calculated using SE, SEP, and CI approximations. The present results have also been compared with those of Varella *et.al.* [22], Nishimura [23] and Kimura *et.al.* [21]. The Q_T values reported by Kimura *et.al.* [21] are in higher values than the present Q_{el}, as expected. Additionally, the current Q_{el} with born, shows reasonable matching with the vibrational Q_{el} of Nishimura [23]. Varella *et.al.* [22] theoretical Q_T (TCS) values for the CH_2F_2 molecule have been also reviewed by Song *et.al.* [39].

B. Intermediate to high energy results

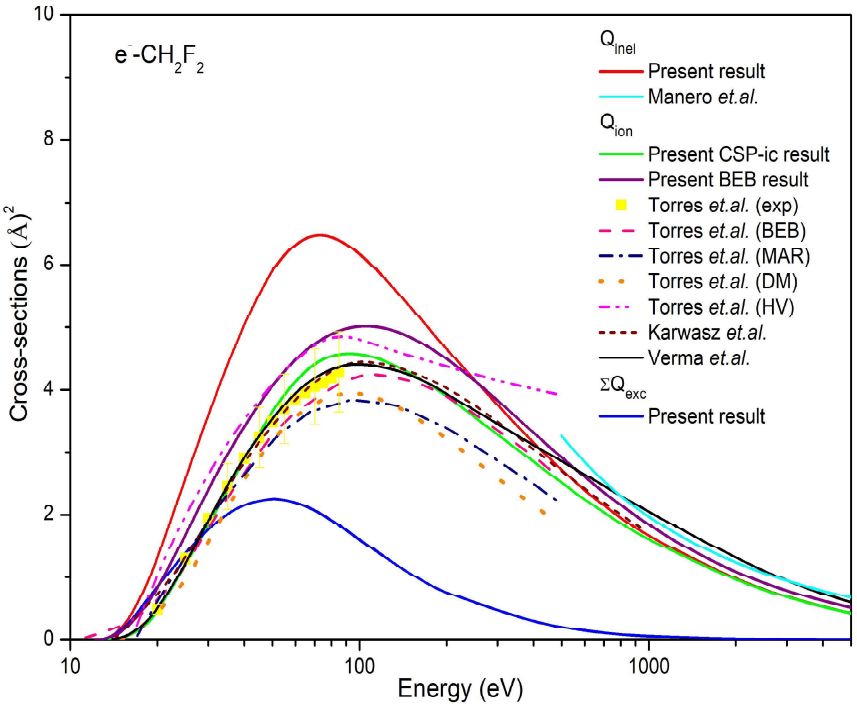

Figure 6.7 Inelastic cross-sections for $e^- - CH_2F_2$ scattering

Red solid: Present Q_{inel}; Green solid: Present Q_{ion} (CSP-ic); Purple solid: Present Q_{ion} (BEB); Yellow filled squares: Torres et.al. measured Q_{ion} [26]*; Pink dash: Torres et.al. Q_{ion} using BEB formalism* [28]*; Navy blue dash dot: Torres et.al. Q_{ion} using MAR method* [26]*; Orange dot: Torres et.al. Q_{ion} using DM formalism* [26]*; Pink dash dot dot: Torres et.al. Q_{ion} using HV method* [26]*; Wine short dash: Karwasz et.al. Q_{ion} using BEB* [27]*; Black solid: Verma et.al. Q_{ion}* [29]

Figure 6.7 shows the present findings for Q_{inel}, Q_{ion}, and Q_{exc} of CH_2F_2 with the available ones. The comparison can be made with the lone Q_{inel} data of Manero *et.al.* [18]. For energy from 500 - 10000 eV, they [18] estimated the Q_{inel} by deducting their Q_{el} values from their Q_T data. Although the present data understates their results statistically, the qualitative matching between them is good [18]. In the present study, Q_{ion} data computed using two distinct methods: BEB and CSP-ic. Torres *et.al.* reported the measured Q_{ion} [26] as well as computed Q_{ion} [28] utilising various approaches, including BEB, DM, Modified additivity rule (MAR), and Harland and Vallance (HV) method for the energy 10-500 eV. The present Q_{ion} exceeds

computed Q_{ion} [28], and measured Q_{ion} (within the indicated uncertainty of 10-20%) [26] of Torres *et.al.* However, the present results have a comparable shape to the experimental and computed data of Torres *et.al.* [26,28]. By employing BEB method, Karwasz *et.al.* [27] has computed Q_{ion} for CH_2F_2 and from the figure 6.7, good matching with the present Q_{ion} can be seen. Verma *et.al.* [29] estimated the Q_{ion} using the CSP-ic approach with the value of $R_p = 0.8$, whereas we used $R_p = 0.7$ in the present work. The modest difference between their result [29] and the present results is assumed to be due to different R_p values. As far as we know, there are no available data for summed $\sum Q_{exc}$.

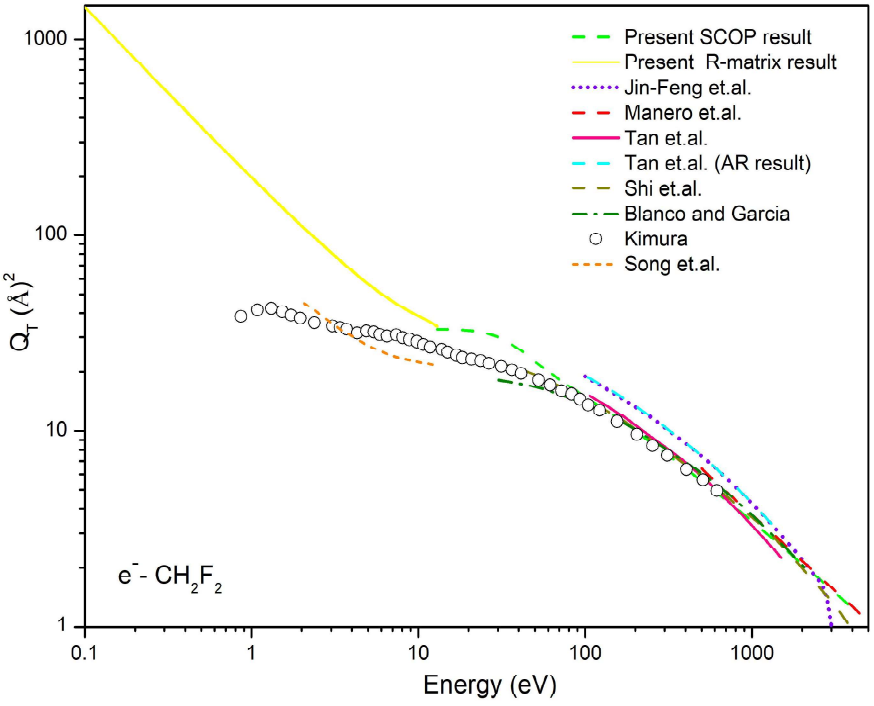

Figure 6.8 Total cross-sections for $e^- - CH_2F_2$ scattering

Yellow solid: Present Q_T (with born); Blue solid: Present Q_T (without born); Orange solid: Present Q_{el} (SCOP result); Green dash dot: Present Q_T (SCOP result); Purple dots: Jin-Feng et.al. Q_T [19]*; Red dash: Manero et.al. Q_T* [18]*; Olive green dash: Manero et.al. Q_{el}* [18]*; Pink solid: Tan et.al. Q_T* [17]*; Cyan dash: AR results of Q_T by Tan et.al.* [17]*; Dark yellow dash: Shi et.al. Q_T* [20]*; Violet dash dot: Blanco and García Q_T* [20]*; Open circles: Kimura et.al. Q_T* [21]*; Orange short dash: Varella et.al. Q_T data, reported by Song et.al.* [39]

In the figure 6.8, the Q_T is plotted against the incoming energy ranging from 0.1 eV to 5000 eV. The Q_T values of Tan *et.al.* [17] (for energy 100-1500 eV) and Jin-Feng *et.al.* [19] (for energy 100-3000 eV) obtained through additivity rule (AR) show the higher values compared to all other available data [18,20,21]. It's possible that this is because the AR approach ignores the effect of multi-centre scattering. Tan *et.al.* [17] then employed a modified AR technique to obtain considerable findings, the results of which overlap with the present ones. Manero *et.al.* [18] estimated the Q_T using a semi-empirical formula for 500-10000 eV, and the current data matches their results extremely well above 100 eV. The results of Shi *et.al.* [20], Blanco and García [20] and Kimura *et.al.* [21] have also shown a similar tendency with the current Q_T values. Above 80 eV, the current data begins to overlap with their [20,21] results. The variation on the lower energy side can be attributed to the adoption of the geometric AR approach, which is not suitable for lower energies [17]. Figure 6.8 shows the excellent matching of the data provided by two independent approaches viz., R-matrix and SCOP.

6.3 Methyl fluoride (CH_3F)

Total, elastic, and inelastic processes for electron scattering from methane and fluoromethane (such as CH_3F) have attracted a lot of attention recently [1] due to the growing importance of understanding the fundamental nature of molecular electronic structures and scattering processes and their applications in plasma chemistry and the material sciences.

In many different types of air conditioning and refrigeration systems, CH_3F is the refrigerant of choice. Because of its favourable thermodynamic qualities, including as its moderate pressure and low boiling point, it is well suited for use in refrigeration equipment. In the production of a wide variety of pharmaceutical chemicals, it is frequently used either as an initial ingredient or as reagent. It is possible to incorporate it into the molecules of a medicine in order to change the properties of the drug, such as making it more bioavailable or metabolically stable. In aerosol products like spray paints and lubricants, it can be found functioning in the capacity of a propellant at times. Because it has such a low boiling point, it can evaporate very quickly, which helps it propel whatever is within the aerosol can. In the semiconductor industry, plasma etching techniques frequently call for the utilization of CH_3F. As a result of its reaction with SiO_2 and other substances, it enables the accurate removal of thin layers during the manufacturing process of microelectronic devices. To make this process

reliable, information on the electron interactions with them are essential in for the plasma etching processes.

It is essential to keep in mind that methyl fluoride is a powerful greenhouse gas, and while utilizing it in a variety of applications, its impact on the surrounding environment should be taken into consideration. To reduce the likelihood of any adverse effects occurring, it is imperative that appropriate handling, storage, and disposal procedures be followed.

6.3.1 Literature study

Table 6.5 shows the previous study on the electron collision cross-sections for CH_3F molecule.

Table 6.5 Literature survey on electron collision study of CH_3F for the reported energy range

Quantity	Energy range	Method	References
Q_{EDCS}	5 - 20 eV	Schwinger multichannel method	Varella *et.al.* [22]
	15 – 500 eV	Complex Optical Potential method	Ferraz *et.al.* [40]
	10 and 20eV	Schwinger Multichannel Method with Pseudopotentials	Natalense *et.al.* [25]
	20 eV	Schwinger multichannel method	Natalense *et.al.* [24]
Q_{el}	0 – 15 eV	Schwinger multichannel method	Varella *et.al.* [22]
	0.3 – 250 eV	Electron Transmission Experiment	Krzysztofowicz and Szmytkowski [41]
	15 – 500 eV	Complex Optical Potential method	Ferraz *et.al.* [40]
Q_{MTCS}	1.5 – 15 eV	Schwinger multichannel method	Varella *et.al.* [22]
	15 – 500 eV	Complex Optical Potential method	Ferraz *et.al.* [40]
	0 – 30 eV	Schwinger	Natalense *et.al.* [24]

		multichannel method	
Q_{inel}	50 – 5000 eV	Optical Potential	Joshipura and Vinodkumar [42]
Q_{ion}	10 – 1000 eV	Review article	Karwasz *et.al.* [27]
	< 100 eV	Mass-resolved TOF spectroscopy and BEB, DM, HV, MAR	Torres *et.al.* [28]
	0 – 180 eV	Total ion current method (no mass selection)	Vallance *et.al.* [43]
	IE – 1000 eV	Using time-of-flight spectrometer	Rejoub *et.al.* [27,44]
	50 – 5000 eV	Optical Potential	Joshipura and Vinodkumar [42]
Q_T	15 – 500 eV	Complex Optical Potential method	Ferraz *et.al.* [40]
	100 – 3000 eV	Additivity rule	Jin-Feng *et.al.* [19]
	30 – 5000 eV		Shi *et.al.* [20]
	300 – 5000 eV	Experimental	Manero *et.al.* [18]
	100 – 1500 eV	Revised additivity rule	Tan *et.al.* [45]
	50 – 5000 eV	Optical Potential	Joshipura and Vinodkumar [42]

6.3.2 Target model

Table 6.6 shows various target properties of CH_3F that were estimated using three distinct scattering models (SE, SEP, and CI) through R-matrix formalism.

Table 6.6 Various target properties of CH_3F calculated using Quantemol-N

Target properties (unit)	**Present (Quantemol-N/6- 311G*)**		
	CAS-CI	**SE**	**SEP**
Ground state energy (Hartree)	-139.0758	-137.5696	-237.9583

Dipole moment (Debye)		1.850	1.850	1.850
Rotational constant (cm^{-1})	A	5.2226	5.2227	5.2227
	B	0.8510	2.3086	2.3086
	C	0.8510	2.3083	2.3083

CH_3F is a C_{3v} symmetric molecule, which is treated as belonging to C_s symmetry. The HF ground state electron configuration for CH_3F employed in this study is $1(a')^2$, $2(a')^2$, $3(a')^2$, $4(a')^2$, $1(a'')^2$, $5(a')^2$, $6(a')^2$, $2(a'')^2$, $7(a')^2$. All 18 electrons are rendered inactive in the lowest setting of the SEP and SE model. For the augmentation of the continuum orbitals in the SE model, the computations incorporate 4 virtual molecular orbitals (MO) of a', and 1 virtual MO of a'' symmetry. The SEP model, on the other hand, retains 25 virtual MO of a', and 11 virtual MO of a''. However, in the CI model, 8 of the 18 electrons are kept frozen in positions 1a', 2a', 3a', and 4a'. The remaining 10 electrons are free to move in the active space of the 8 molecular occupied and virtual orbitals 5a', 6a', 7a', 8a', 9a', 1a'', 2a'', 3a''. Five virtual MOs are assigned to improve the continuum orbitals, four of which retain a' symmetry and one of which retains a'' symmetry. To obtain more precise calculations, for ground state representation, 606 configuration state functions (CSFs) and for close coupling expansion and outer regime calculation, 5 target states are used. The first 5 excited states are tabulated in Table 6.7 for CH_3F molecule.

Table 6.7 Vertical excitation energies for all states of CH_3F

	States	**Energy (eV)**
Singlet	a'	0
Triplet	a'	11.2677
Triplet	a''	11.2704
Singlet	a'	11.8255
Singlet	a''	11.8282

The target parameters which are used in the calculation of high energies through SCOP, are listed below in table 6.8.

Table 6.8 Properties of CH_3F [33]

Properties	Values
Ionisation energy (eV)	12.50
Polarisability ($Å^3$)	2.54
Bond length (Å)	C-H = 1.0818 C-F = 1.3646

6.3.3 Results and Discussion

We conducted a thorough study of the electron collision cross section for the CH_3F for impact energies ranging from 0.1 eV to 5000 eV by employing R-matrix and SCOP formalisms to compile a comprehensive database.

A. Low energy results

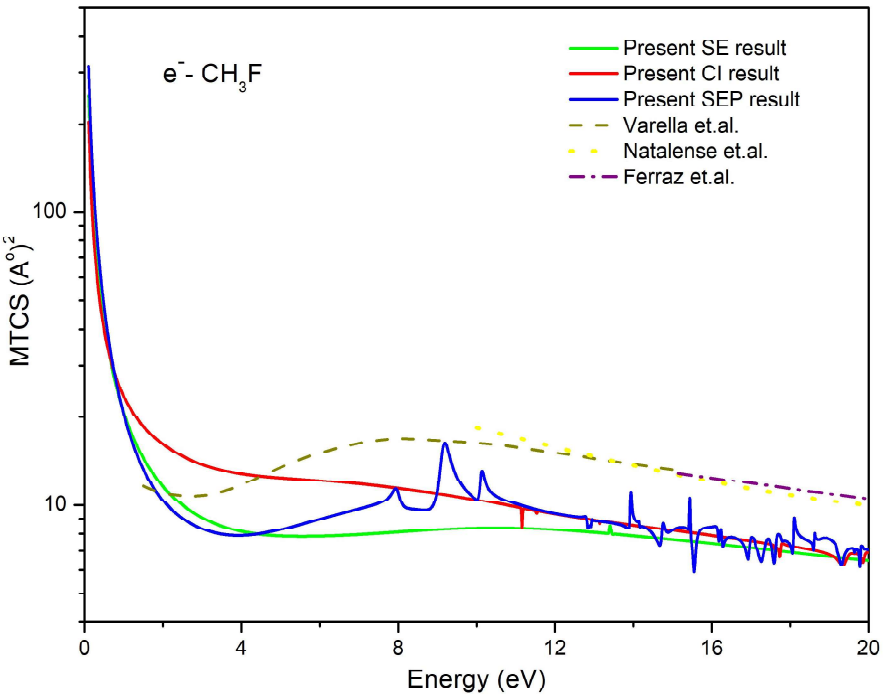

Figure 6.9 Q_{MTCS} for $e^- - CH_3F$ scattering

Green solid: Present SE result; red solid: Present CI result; blue solid: Present SEP result; dark yellow dash: Varella et.al. [22]*; yellow dot: Natalense et.al.* [24]*; purple dash dot: Ferraz et.al.* [40]

Figure 6.9 compares the current Q_{MTCS}, computed using three distinct models: SE, SEP, and CI, to the results of Varella *et.al.* [22], Ferraz *et.al.* [40] and Natalense *et.al.* [24] for energies 0.1 to 20 eV. The present Q_{MTCS} data underestimates all existing results [22,24,40].

Figure 6.10 depicts the present Q_{EDCS} data for CH_3F for energies of 5 eV and 10 eV. As seen earlier in case of CH_2F_2, the Q_{EDCS} of CH_3F is also rising rapidly at small angles, resulting in a noticeable forward peak, a feature due to the polar molecules' long-range dipole interactions. At the energy of 5 eV, the only existing data for Q_{EDCS} is of Varella *et.al.* [22]. The current data is consistent with the experimental and theoretical SEP results of Varella *et.al.* [22] within the specified uncertainty range of ±15-20% for $\theta < 80°$. Varella *et.al.* [22] theoretical data utilising the SE technique are seen minutely higher than the current ones at forward angle regime. They also overestimate the findings calculated using their SEP model.

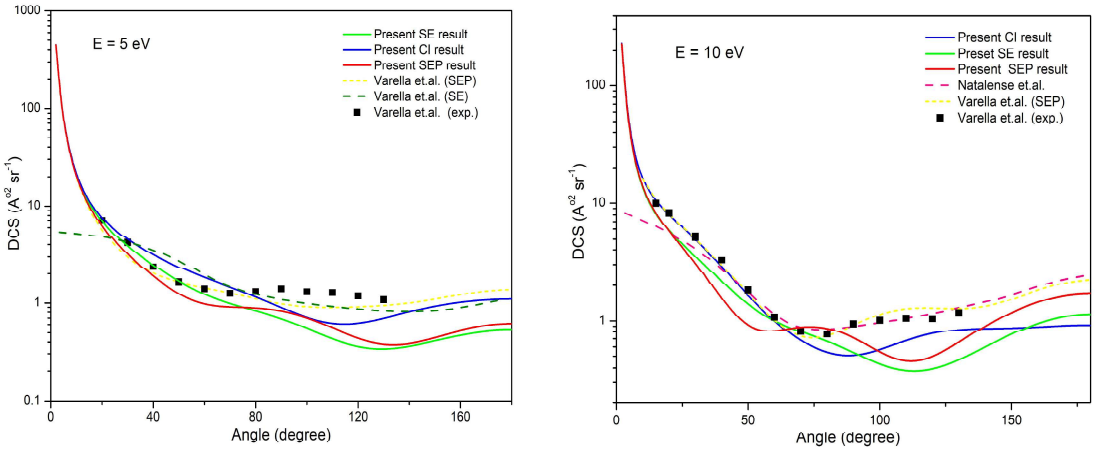

Figure 6.10 Q_{EDCS} at 5 eV and 10 eV energy for e^- - CH_3F scattering

Green solid: Present SE result; blue solid: Present CI result; red solid: Present SEP result; yellow short dash: Varella et.al. SEP result [22]*; olive green dash: Varella et.al. SE result* [22]*; filled squares: Varella et.al. (exp.)* [22]*; pink dash: Natalense et.al.* [24]

However, for 10 eV, the current values of Q_{EDCS} correspond well with the results of Varella *et.al.* [22] and Natalense *et.al.* [24]. The mismatch between the Natalenlense *et.al.* data and the present result at higher angles is may be due to the fact as mentioned earlier in case of CH_2F_2 also, that Natalense *et. al.* [24] did not account for the polarisation effect, despite the fact that CH_3F has a permanent dipole moment of 1.850 debye, which has the main influence in Q_{EDCS} at small angles, as previously indicated. Furthermore, the 5 eV and 10 eV figures

display two broad minima, indicating the presence of *d*-wave structure, which is absent in all of the data of Varella *et. al.* [22].

In figure 6.11, Q_{el} results for CH_3F has been plotted and compared with the available data of Varella *et.al.* [22], Krzysztofowicz and Szmytkowski [41] and Ferraz *et.al.* [40]. Both SE and SEP results of Varella *et.al.* [41] are seen to be in very good accord with the present Q_{el} data. The experimental results of Krzysztofowicz and Szmytkowski [41] is also in excellent agreement with the present ones, except for the intermediate energy regime. Ferraz *et.al.* [40] has reported the Q_{el} for energies 15 – 500 eV. For the present energy regime (0.1 – 20 eV), their results overestimate both the results: present ones and that of Varella *et.al.* [22].

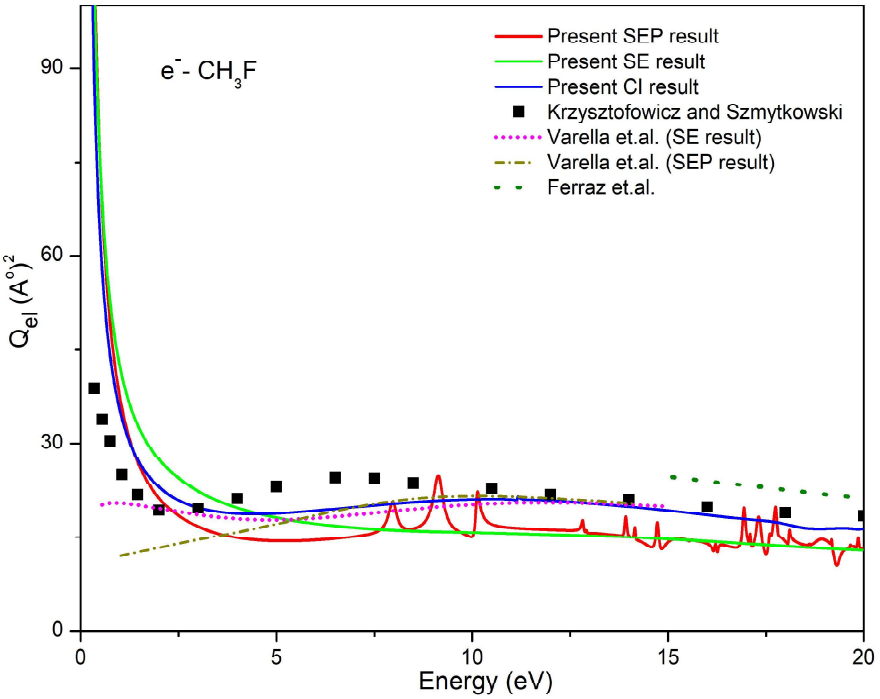

Figure 6.11 Q_{el} for e^- - CH_3F scattering

Red solid: Present SEP result; green solid: Present SE result; blue solid: Present CI result; dark yellow dash dot: Varella et.al. (SEP result) [22]*; magenta short dot: Varella et.al. (SE result)* [22]*; olive green dot: Ferraz et.al.* [40]*; filled squares: Krzysztofowicz and Szmytkowski* [41]

B. Intermediate to high energy results

Figure 6.12 depicts the results of inelastic interaction cross-sections for energies, ranging from ionisation energy of CH_3F to 5000 eV. The present Q_{inel} result is compared with that of Joshipura and Vinodkumar [42] and can be seen that present Q_{inel} and Q_{ion} underestimates that of Joshipura and Vinodkumar [42]. One of the reasons for this mismatch can be the use of modified additivity rule-screening correction (MAR-SC) by them [42].

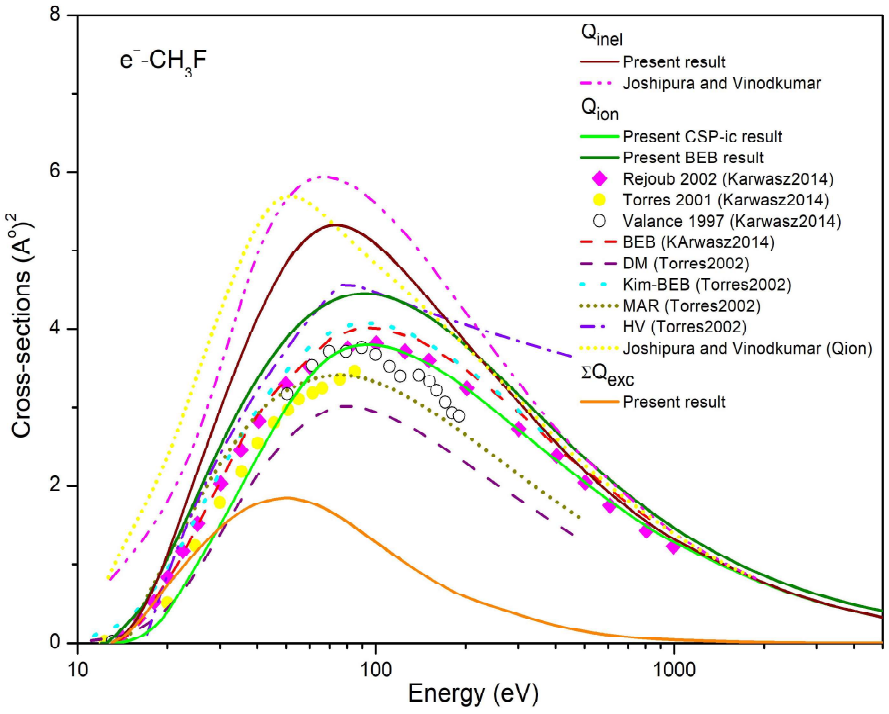

Figure 6.12 Inelastic cross-sections for $e^- - CH_3F$ scattering

Wine solid: Present Q_{inel}; magenta dash dot dot: Joshipura and Vinodkumar Q_{inel} [42]*; green solid: Present Q_{ion} (CSP-ic result); olive green solid: Present Q_{ion} (BEB result); filled rotated squares: Rejoub et.al.* [27,44] *Q_{ion}; filled circles: Torres et.al. Q_{ion}* [28]*; open circles: Vallance et.al. Q_{ion}* [43]*; red dash: Karwasz et.al. Q_{ion}* [27]*; purple dash: Torres et.al. Q_{ion} (DM method)* [28]*; cyan dot: Torres et.al. Q_{ion} (Kim-BEB method)* [28]*; dark yellow short dot: Torres et.al. Q_{ion} (MAR method)* [28]*; violet dash dot: Torres et.al. Q_{ion} (HV method)* [28]*; yellow short dot: Joshipura and Vinodkumar Q_{ion}* [42]*; orange solid: Present ΣQ_{exc}*

Present Q_{ion} data computed through BEB and CSP-ic are also plotted in figure 6.12. Torres *et.al.* reported computed Q_{ion} [28] utilising various approaches, including BEB, DM,

Modified additivity rule (MAR), and Harland and Vallance (HV) method for the energy 10 - 500 eV. The present CSP-ic result can be seen in excellent agreement with that of Rejoub *et.al.* [27,44], Torres *et.al.* [28], Vallance *et.al.* [43].

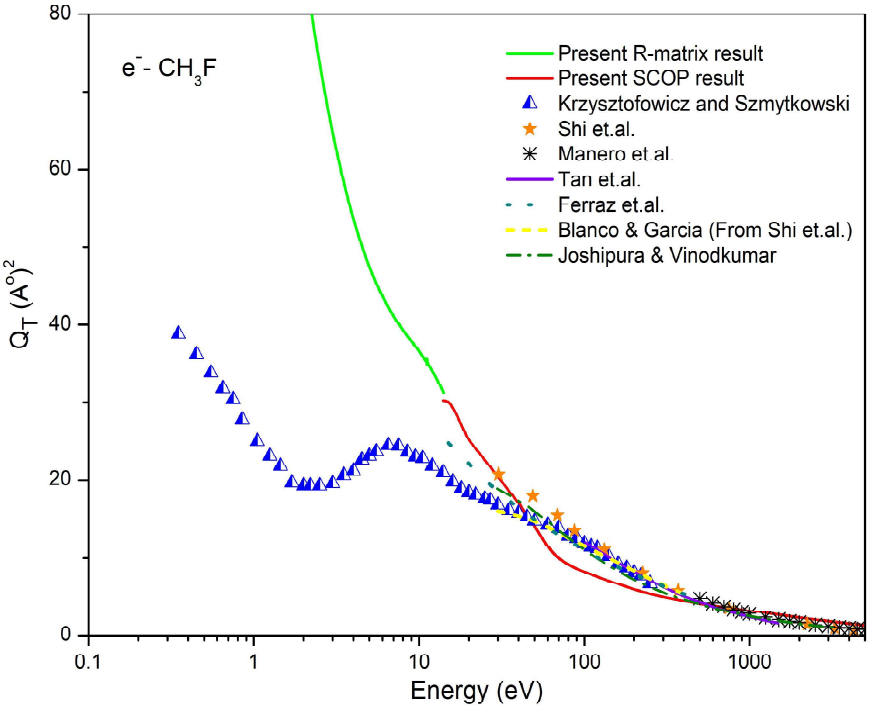

Figure 6.13 Total cross-sections for e^- − CH_3F scattering

Green solid: Present R-matrix Q_T; red solid: Present SCOP Q_T; half-filled triangles: Krzysztofowicz and Szmytkowski [41]*; filled stars: Shi et.al.* [20]*; asterisk: Manero et.al.* [18]*; violet solid: Tan et.al.* [45]*; dark cyan dot: Ferraz et.al.* [40]*; yellow short dash: Blanco and Garcia* [46]*; olive green dash dot: Joshipura and Vinodkumar* [42]

In the figure 6.13, the Q_T is plotted for the energy range, 0.1 eV to 5000 eV. From figure a smooth connection between the results obtained through both the methodologies: R-matrix and SCOP can be observed. We have compared our high energy result of Q_T with the available data [20,40,42,45–47]. The comparison of low energy results can be seen in figure 6.11. At the intermediate energies (50 - 400 eV) the discrepancy between the present result and available ones can be observed. However, the present SCOP result can be seen in good agreement with all the existing ones at energies higher than 400 eV.

6.4 Bibliography

[1] L. G. Christophorou. J. K. Olthoff, and M. V. V. S. Rao, *Electron Interactions with CF4*, Journal of Physical and Chemical Refernce Data **25**, 1341 (1996).

[2] H. Tanaka, T. Masai, M. Kimura, T. Nishimura, and and Y. Itikawa, *Fluorination Effects in Electron Scatterings from CH4, CH3F1, CH2F2, CH1F3 , and CF4*, Phys Rev A (Coll Park) **56**, 3338 (1997).

[3] S. J. Moss and A. Ledwith, (editors), *The Chemistry of Semiconductor Industry* (Blackie, Glasglow, New York, 1987).

[4] N. H. and K. M. Edited by J.T. Houghton, L.G. Meira Filho, J. Bruce, Hoesung Lee, B.A. Callander, E. Haites, Intergovernmental Panel in Climate Change (IPCC), 1995.

[5] U. S. Environmental Protection Agency, National Air Pollutant Emissions Trends Report, 1998, 2000.

[6] S. Arulmozhiraja and T. Fujii, *Li+ Ion Affinities of Global-Warming Perfluorocarbons*, Journal of Physical Chemistry A **104**, 9613 (2000).

[7] *Hydrofluorocarbons (HFCs)*, https://www.ccacoalition.org/en/slcps/hydrofluorocarbons-hfcs.

[8] T. and E. A. P. UNEP, TEAP 2010 PROGRESS REPORT, n.d.

[9] GHG Protocol, *Global Warming Potential Values*, https://www.ghgprotocol.org/sites/default/files/ghgp/Global-Warming-Potential-Values%28Feb 16 2016%29_1.pdf.

[10] G. A. Longo, S. Mancin, G. Righetti, and C. Zilio, *HFC32 Vaporisation inside a Brazed Plate Heat Exchanger (BPHE)*, Refrigeration Science and Technology **57**, 1187 (2015).

[11] *Difluoromethane*, https://en.wikipedia.org/wiki/Difluoromethane#cite_ref-12.

[12] P. Blowers and K. Hollingshead, *Estimations of Global Warming Potentials from Computational Chemistry Calculations for CH 2F 2 and Other Fluorinated Methyl Species Verified by Comparison to Experiment*, Journal of Physical Chemistry A **113**, 5942 (2009).

[13] *Stratospheric Ozone Protection: The Montreal Protocol and Title VI of the Clean Air Act Amendments of 1990*, Air & Waste **43**, 1066 (1993).

[14] J. Lee, A. Efremov, and K. H. Kwon, *On the Relationships between Plasma Chemistry, Etching Kinetics and Etching Residues in CF4+C4F8+Ar and CF4+CH2F2+Ar Plasmas with Various CF4/C4F8 and CF4/CH2F2 Mixing Ratios*, Vacuum **148**, 214 (2018).

[15] Y. C. Sung, T. C. Wei, Y. C. Liu, and C. Huang, *Silicon Etching of Difluoromethane Atmospheric Pressure Plasma Jet Combined with Its Spectroscopic Analysis*, Jpn J Appl Phys **57**, (2018).

[16] Catherine B. Labelle, Kenneth K.S. Lau, Karen K. Gleason, *Pulsed Plasma Enhanced Chemical Vapor Deposition from CH2F2, C2H2F4, and CHCIF2*, Materials Research Society Symposium Proceedings **511**, 75 (1998).

[17] X. M. Tan and G. Zhao, *Total Cross Sections for Electron Scattering from Fluoromethanes: A Revised Additivity Rule Method*, Chinese Physics B **21**, (2012).

[18] F. Manero, F. Blanco, and G. García, *Electron-Scattering Cross Sections of Fluoromethanes in the Energy Range from 0.1 to 10 KeV*, Phys Rev A **66**, 327131 (2002).

[19] J. F. Sun, X. M. Tan, Y. F. Liu, and D. H. Shi, *Total Cross Sections for Electron Scattering from CF4, CF 3H, CF2H2, and CFH3 Molecules in Energy Range from 100 to 3000 EV*, Commun Theor Phys **42**, 267 (2004).

[20] D. Shi, Y. Liu, J. Sun, H. Ma, and Z. Zhu, *Geometric Shielding Corrections for Calculation of Electron Scattering by CO2, C2H2, CHCl3, CH2Cl2, CH3Cl, CHF3, CH2F2 and CH3F at 30-5000 EV*, Radiation Physics and Chemistry **77**, 528 (2008).

[21] M. Kimura, *A COMPARATIVE STUDY OF ELECTRON- AND POSITRON-POLYATOMIC MOLECULE* (n.d.).

[22] M. T. do N. Varella, C. Winstead, V. McKoy, M. Kitajima, and H. Tanaka, *Low-Energy Electron Scattering by CH3F, CH2F2, CHF3, and CF4*, Phys Rev A **65**, 22702/1 (2002).

[23] T. Nishimura, *Theoretical Study of Electron Scattering from CH2F2 Molecules*, Journal of Physics B: Atomic, Molecular and Optical Physics **31**, 3471 (1998).

[24] Alexandra P. P. Natalense, Márcio H. F. Bettega, Luiz G. Ferreira,1, and Marco A. P. Lima, *Halogenation Effects in Electron Scattering from CHF3, CH2F2, CH3F, CHCl3, CH2Cl2, CH3Cl, CFCl3, CF2Cl2, and CF3Cl*, Phys Rev A **59**, (1999).

[25] Alexandra P. P. Natalense, Marcio T. do N. Varella, Marcio H. F. Bettega, Luiz G. Ferreira, and Marco A. P. Lima, *Applications of the Schwinger Multichannel Method with Pseudopotentials to Electron Scattering from Polyatomic Molecules I. Elastic Cross Sections*, Brazilian Journal of Physics **31**, (2001).

[26] I. Torres, R. Martínez, M. N. Sánchez Rayo, and F. Castaño, *Electron Impact Dissociative Ionization of the CH2F2 Molecule: Cross Sections, Appearance Potentials, Nascent Kinetic Energy Distributions and Dissociation Pathways*, Journal of Physics B: Atomic, Molecular and Optical Physics **33**, 3615 (2000).

[27] Grzegorz P. karwasz. Pawel Mozejko, and Mi-Young Song, *Electron-Impact Ionization of Fluoromethanes – Review of Experiments and Binary-Encounter Models*, Inkrnarional Journal of Mass Spectrometry **365–366**, 232 (2014).

[28] I. Torres, R. Martínez, M. N. Sánchez Rayo, and F. Castaño, *Evaluation of the Computational Methods for Electron-Impact Total Ionization Cross Sections: Fluoromethanes as Benchmarks*, Journal of Chemical Physics **115**, 4041 (2001).

[29] P. Verma, R. Naghma, and B. Antony, *Electron Impact Ionisation Cross Sections Derived from Total Inelastic Cross Section for CF3X and CF2X2 (X = H, Cl, Br and I) Molecules*, Mol Phys **114**, 1778 (2016).

[30] Y. Itikawa, *The Born Closure Approximation for the Scattering Amplitude of an Electron-Molecule Collision*, Theor Chem Acc **105**, 123 (2000).

[31] S.-I. Chu and A. Dalgarno, *Rotational Excitation of C H + by Electron Impact*, Phys Rev A (Coll Park) **10**, 788 (1974).

[32] C. R. Brundle, M. B. Robin, and H. Basch, *Electronic Energies and Electronic Structures of the Fluoromethanes*, J Chem Phys **53**, 2196 (1970).

[33] R. D. Johnson, *Experimental Data for CH2F2*, https://cccbdb.nist.gov/exp2x.asp?casno=75105&charge=0.

[34] R. D. Amos, N. C. Handy, W. H. Green, D. Jayatilaka, A. Willetts, and P. Palmieri, *Anharmonic Vibrational Properties of CH2F2: A Comparison of Theory and Experiment*, Journal of Chemical Physics **95**, 8323 (1991).

[35] J. A. Koutcher, R. H. Larkin, J. R. Williams, and S. G. Kukolich, *Rotational Absorption Spectrum of Methylene Fluoride in the 20-100 Cm-1 Region*, J Mol Spectrosc **60**, 373 (1976).

[36] E. Hirota, T. Tanaka, A. Sakakibara, Y. Ohashi, and Y. Morino, *Microwave Spectrum of Methylene Fluoride Centrifugal Distortion and Molecular Structure*, J Mol Spectrosc **34**, 222 (1970).

[37] J. Tennyson, *Electron-Molecule Collision Calculations Using the R-Matrix Method*, Phys Rep **491**, 29 (2010).

[38] T. Jani, H. Yadav, D. Prajapati, P. C. Vinodkumar, and M. Vinodkumar, *Theoretical Investigation of Electron Impact on Formyl Fluoride (HFCO)*, Radiation Physics and Chemistry **177**, 109098 (2020).

[39] M. Y. Song, J. S. Yoon, H. Cho, G. P. Karwasz, V. Kokoouline, Y. Nakamura, and J. Tennyson, *"Recommended" Cross Sections for Electron Collisions with Molecules*, European Physical Journal D **74**, (2020).

[40] J. R. Ferraz, A. S. Dos Santos, G. L. C. De Souza, M. T. Lee, L. M. Brescansin, R. R. Lucchese, and L. E. Machado, *Cross Sections for Electron Scattering by Methylfluoride (CH3F) in the Low- and Intermediate-Energy Ranges*, J Electron Spectros Relat Phenomena **193**, 16 (2014).

[41] C. Szmytkowski, *Electron-Methyl Halides Scattering. Total Cross Section Measurements for Methyl Chloride and Methyl Fluoride*, Journal of Physics B: Atomic, Molecular and Optical Physics **28**, 1593 (1995).

[42] K. N. Joshipura and M. Vinodkumar, *Various Total Cross-Sections for Electron Impact On*, The European Physical Journal D **5**, 229 (1999).

[43] C. Vallance, S. A. Harris, J. E. Hudson, and P. W. Harland, *Absolute Electron Impact Ionization Cross Sections for , Where* **X** *= H, F, Cl, Br, and I*, Journal of Physics B: Atomic, Molecular and Optical Physics **30**, 2465 (1997).

[44] R. Rejoub; B. G. Lindsay; R. F. Stebbings, *Electron-Impact Ionization of the Methyl Halides*, J Chem Phys **117**, 6450 (2002).

[45] Tan Xiao-Ming and Gang Zhao, *Total Cross Sections for Electron Scattering from Fuoromethanes: A Revised Additivity Rule Method*, Chinese Physics B **21**, 063402 (2012).

[46] F. Manero, F. Blanco, and G. García, *Electron-Scattering Cross Sections of Fluoromethanes in the Energy Range from 0.1 to 10 KeV*, Phys Rev A **66**, 327131 (2002).

[47] G. P. Karwasz, P. Mozejko, and M. Y. Song, *Electron-Impact Ionization of Fluoromethanes - Review of Experiments and Binary-Encounter Models*, Int J Mass Spectrom **365–366**, 232 (2014).